Analysis of Irregularities in a Planar Dielectric Waveguide

SHYH-JONG CHUNG AND CHUN HSIUNG CHEN

Abstract—**A numerical method based on the partial variational principle (PVP) is proposed to solve discontinuity problems due to arbitrary irregularities in a planar dielectric waveguide. In this study, a variational equation is established and solved by the finite element method along with the Green's function technique. The integral variable of the Green's function is changed so that numerical calculations can easily be performed. Owing to the accuracy of the present method, the radiation fields can be obtained with no difficulty. Several numerical results, including the reflection and transmission coefficients as well as the radiation losses and patterns, are calculated and compared.**

I. Introduction

DISCONTINUITY problems in open dielectric waveguides are essential to the design of various optical and millimeter-wave components, such as filters, grating couplers, and distributed feedback lasers. They also play an important role in the splicing of two optical fibers. Because of the unboundedness of the structure and the presence of the continuous spectrum, the analysis of the discontinuities in an open waveguide is more difficult than that in a closed one. Roughly speaking, the discontinuity problems in open waveguides may be divided into three categories: problems with small discontinuities, problems with step discontinuities, and problems with arbitrary discontinuities.

For the first category, Marcuse [1] approximated a tapered dielectric waveguide by many infinitesimal step junctions, and then assumed that the modes of the adjacent waveguides are approximately orthogonal. Clarricoats and Sharpe [2] neglected the continuous modes and matched only the discrete modes at the junction of a small step. Miyanaga and Asakura [3] solved a linearly tapered grating coupler on the basis of the first-order perturbation theory by dividing the grating region into short subsections.

For problems with large steps, some authors have replaced the unbounded configuration by bounded [4] or periodic [5] ones. Some have discretized the continuous spectrum of the radiation modes, using a complete set of "good functions" for expansion [6]–[8]. They then applied the mode-matching technique or the least squares boundary residual method to solve the step discontinuities. Rozzi and In'tVeld [9]–[11] solved an integral equation by the Ritz–Galerkin method, while Gelin *et al.* [12] and Capsalis *et al.* [13] solved it by the Neumann series iteration procedure.

The previous methods can solve discontinuity problems either with slight perturbations or with regular shapes, such as step junction problems. It appears that none of these methods can be used to tackle problems with arbitrary discontinuities. Suzuki and Koshiba [14] treated these problems by combining the finite element method and the analytical method. In their work, the fields far from the waveguide discontinuities were assumed to be zero; thus one could place a semi-infinite electric conductor at the field-free region.

In our approach, the scattering problem of a uniform slab waveguide with arbitrary discontinuities is analyzed on the basis of the partial variational principle (PVP) [15]. From the PVP, a variational equation including the interior and exterior fields is obtained and solved by the finite element method coupled with the frontal solution technique [16]. The interior fields are represented by the finite element nodal values and the corresponding local bases, while the exterior fields are expanded as a function of the nodal values at the discontinuity region through the Green's function of the uniform slab waveguide. Since no assumption about the fields far from the discontinuities is imposed, the finite element boundary can be put as close to the irregular region as possible.

The validity of the proposed method is examined by observing the convergence and the power conservation of the numerical data, and also by comparing the numerical results with those obtained by other methods. The reflection and transmission coefficients as well as the radiation patterns caused by several discontinuities are presented and compared.

II. Formulation of the Problem

A. Variational Equation

In this study, we consider only the symmetric discontinuity problems associated with a slab waveguide which is excited by an even TE mode as shown in Fig. 1(a). The structure is symmetric with respect to the $y-z$ plane and is uniform in the y direction. Thus an infinite magnetic wall Γ_0 may be placed on the $y-z$ plane so that only the

Manuscript received January 2, 1988; revised April 13, 1988. This work was supported by the National Science Council of the Republic of China under Grant NSC 77-0404-E002-01

The authors are with the Department of Electrical Engineering, National Taiwan University, Taipei, Taiwan, R.O C

IEEE Log Number 8822157

0018-9480/88/0900-1352$01.00 ©1988 IEEE

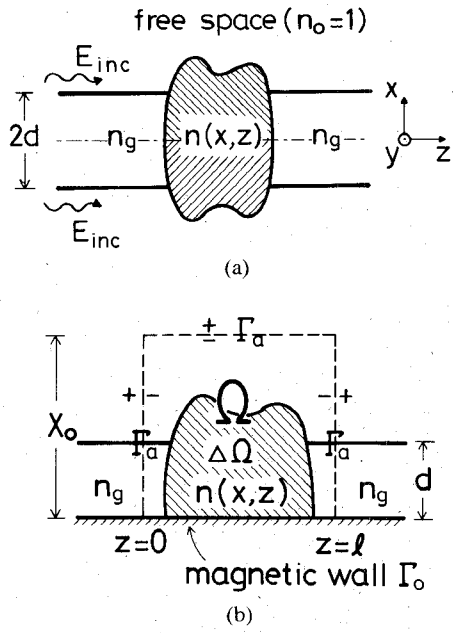

Fig. 1. (a) Original scattering problem with irregularities in slab waveguide. (b) Half structure for analysis.

region $x \geq 0$ needs to be considered. Then we have an irregular region $\Delta\Omega$ of arbitrary shape and inhomogeneous refractive index $n(x, z)$ connected to an otherwise uniform slab guide of refractive index n_g and half-width d, as shown in Fig. 1(b). The magnetic wall Γ_0 and the artificial boundary Γ_a enclose the finite element region Ω ($0 \leq z \leq l$, $0 \leq x \leq X_0$).

From the partial variational principle (PVP) [15], one gets the following variational equation:

$$\delta^a I^a = 0$$

$$I^a = \int_\Omega dv \left[\boldsymbol{E}^a \cdot (\boldsymbol{J} - \boldsymbol{J}_0) - \boldsymbol{H}^a \cdot (\boldsymbol{M} - \boldsymbol{M}_0)\right] + \int_\Gamma ds \left[\boldsymbol{E}^a(\Gamma^-) \cdot (\boldsymbol{K} - \boldsymbol{K}_0) - \boldsymbol{H}^a(\Gamma^+) \cdot (\boldsymbol{N} - \boldsymbol{N}_0)\right] \quad (1)$$

where $\Gamma = \Gamma_a + \Gamma_0$ ($0 \leq z \leq l$). Here, $\boldsymbol{J}_0$ ($\boldsymbol{M}_0$) and $\boldsymbol{K}_0$ ($\boldsymbol{N}_0$) are the impressed electric (magnetic) volume and surface currents, respectively. $(\boldsymbol{E}^a, \boldsymbol{H}^a)$ are the test fields, which may be regarded as a set of weighting functions. The undetermined trial fields $(\boldsymbol{E}, \boldsymbol{H})$ are supported by the sources $\boldsymbol{J}$, $\boldsymbol{M}$, $\boldsymbol{K}$, and $\boldsymbol{N}$ through the relations

$$\boldsymbol{J} = \nabla \times \boldsymbol{H} - j\omega\epsilon_0 n^2 \boldsymbol{E} \quad (2)$$

$$\boldsymbol{M} = -\nabla \times \boldsymbol{E} - j\omega\mu_0 \boldsymbol{H} \quad (3)$$

$$\boldsymbol{K} = \hat{n} \times [\boldsymbol{H}(\Gamma^+) - \boldsymbol{H}(\Gamma^-)] \quad (4)$$

$$\boldsymbol{N} = -\hat{n} \times [\boldsymbol{E}(\Gamma^+) - \boldsymbol{E}(\Gamma^-)]. \quad (5)$$

Here μ_0 and ϵ_0 are the permeability and permittivity of free space, and $\hat{n}$ denotes the outward normal of the boundary Γ whose inner and outer sides are represented by Γ^- and Γ^+, respectively. It is noticed that the partial variational operator δ^a operates only on the test fields with superscript a [15].

Let a TE dominant mode be incident upon the discontinuities from $z = -\infty$; thus the excited fields contain only E_y, H_x, and H_z components. Casting this into (2)–(5) and (1), imposing the constraint $\boldsymbol{M} = \boldsymbol{M}_0 = 0$ in Ω so that the interior magnetic field can be expressed in terms of the interior electric field through (3), and remembering that $\boldsymbol{J}_0$, $\boldsymbol{M}_0$, $\boldsymbol{K}_0$, and $\boldsymbol{N}_0$ are all null, one obtains

$$I^a = \frac{j}{\omega\mu_0} \int_\Omega dv \left[\frac{\partial E_y^a}{\partial x}\frac{\partial E_y}{\partial x} + \frac{\partial E_y^a}{\partial z}\frac{\partial E_y}{\partial z} - k_0^2 n^2 E_y^a E_y\right] + \int_\Gamma ds\, \hat{n} \cdot \left[\hat{z}H_x^a(\Gamma^+) - \hat{x}H_z^a(\Gamma^+)\right]\left[E_y(\Gamma^-) - E_y(\Gamma^+)\right] - \int_\Gamma ds E_y^a(\Gamma^-)\hat{n} \cdot \left[\hat{x}H_z(\Gamma^+) - \hat{z}H_x(\Gamma^+)\right]. \quad (6)$$

As usual, $k_0 = \omega\sqrt{\mu_0\epsilon_0}$ is the propagation constant of free space.

Equation (6) will be solved by the finite element method. The interior fields (E_y^a, E_y) in Ω and $(E_y^a(\Gamma^-), E_y(\Gamma^-))$ are represented by the finite element nodal values and the corresponding local bases. The exterior fields $E_y(\Gamma^+)$, $H_x(\Gamma^+)$, $H_z(\Gamma^+)$, $H_x^a(\Gamma^+)$, and $H_z^a(\Gamma^+)$, which must satisfy the source-free Maxwell's equations outside Ω and the boundary conditions on $\Gamma_0(z < 0,\ z > l)$, will be related to the interior electric fields in the following section.

B. Exterior Field Representation

The transverse fields E_y and H_x can be expanded by the modes of the uniform dielectric waveguide [17], i.e.,

$$E_y = \sum_\nu (a_\nu + b_\nu) u_\nu(x) + \int_0^\infty d\rho\, (a_\rho + b_\rho) u_\rho(x) \quad (7)$$

$$H_x = \sum_\nu (-a_\nu + b_\nu) Y_{0\nu} u_\nu(x) + \int_0^\infty d\rho\, (-a_\rho + b_\rho) Y_{0\rho} u_\rho(x). \quad (8)$$

Here $u_\nu(x)$ and $u_\rho(x)$ are the modal functions for the guided and radiation modes of the uniform waveguide, whose propagation constants are β_ν and β_ρ and whose admittances are $Y_{0\nu}$ ($=\beta_\nu/\omega\mu_0$) and $Y_{0\rho}$ ($=\beta_\rho/\omega\mu_0$), respectively. The modal coefficients (a_ν, a_ρ) and (b_ν, b_ρ), which are functions of z, belong to the modes propagating along the $+z$ and $-z$ directions, respectively.

The transverse fields are the combinations of the incident fields and the scattered fields due to the induced polarization source $j\omega\boldsymbol{P}$ in the irregular region $\Delta\Omega$. The relation between $\boldsymbol{P}$ and $\boldsymbol{E}$ is

$$\boldsymbol{P}(x, z) = (\epsilon(x, z) - \epsilon_b(x))\boldsymbol{E} = \hat{y}\Delta\epsilon E_y = \hat{y}P(x, z) \quad (9)$$

where $\epsilon(x, z)$ and $\epsilon_b(x)$ denote the permittivities with and without the irregularities, respectively, and

$$\Delta\epsilon = \epsilon - \epsilon_b = \epsilon_0 \cdot \begin{cases} n^2(x, z) - n_g^2, & x \leq d \\ n^2(x, z) - 1, & x > d. \end{cases} \quad (10)$$

By the modal orthogonality property and the Lorentz reciprocity relationship, the coefficients in (7) and (8) may

be written as [17] (see the Appendix)

$$a_\mu(z) = a_\mu(0)e^{-j\beta_\mu z} - \frac{j\omega}{2Y_{0\mu}}\int_0^z dz' \int_0^{X_0} dx' P(x', z') u_\mu(x') e^{-j\beta_\mu(z-z')} \tag{11}$$

$$b_\mu(z) = b_\mu(l)e^{j\beta_\mu(z-l)} - \frac{j\omega}{2Y_{0\mu}}\int_z^l dz' \int_0^{X_0} dx' P(x', z') u_\mu(x') e^{j\beta_\mu(z-z')}. \tag{12}$$

Here $u_\mu(x)$ denotes the modal function of either the guided or the radiation mode, and β_μ and $Y_{0\mu}$ are the corresponding propagation constant and admittance, respectively.

The first terms of (11) and (12) are the modal coefficients of the $+z$ and $-z$ propagated modes, respectively, in the absence of the irregularities. The quantities $a_\mu(0)$ and $b_\mu(l)$ are the coefficients of incident modes, which come from $z=-\infty$ and $+\infty$, at $z=0$ and $z=l$, respectively. For the present analysis,

$$a_\mu(0) = \begin{cases} 1, & \mu = 1 \\ 0, & \mu \neq 1 \end{cases} \tag{13}$$

and

$$b_\mu(l) = 0 \qquad \text{for all } \mu. \tag{14}$$

Now by substituting (11) and (12) into (7), one gets

$$E_y(x, z) = u_1(x)e^{-j\beta_1 z} + j\omega \iint_{\Delta\Omega} dx' dz' P(x', z') G(x, z; x', z') \tag{15}$$

where the Green's function G takes the form

$$G(x, z; x', z') = G_1 + G_2 \tag{16}$$

$$G_1(x, z; x', z') = -\frac{1}{2}\sum_\nu \frac{1}{Y_{0\nu}} u_\nu(x) u_\nu(x') e^{-j\beta_\nu|z-z'|} \tag{17}$$

$$G_2(x, z; x', z') = \int_0^\infty d\rho \frac{e^{-j\beta_\rho|z-z'|}}{Y_{0\rho}} u_\rho(x) u_\rho(x'). \tag{18}$$

The integral in (18) can further be separated into two parts: one contains the Green's function of free space, and the other is the additional term due to the presence of the slab [11], i.e.,

$$G_2 = \frac{\omega\mu_0}{2}\left[H_0^{(2)}(k_0R_+) + H_0^{(2)}(k_0R_-)\right] + \omega\mu_0\int_0^\infty d\rho \frac{e^{-j\sqrt{k_0^2-\rho^2}|z-z'|}}{\sqrt{k_0^2-\rho^2}} t(\rho; x, x') \tag{19}$$

where $R_\pm = [(x \pm x')^2 + (z-z')^2]^{1/2}$ and

$$t(\rho; x, x') = u_\rho(x)u_\rho(x') - \frac{2}{\pi}\cos(\rho x)\cos(\rho x'). \tag{20}$$

For numerical computation, the variable ρ in (19) is transformed into a complex variable φ:

$$\rho(\varphi) = k_0 \cos\varphi. \tag{21}$$

Thus (19) becomes

$$G_2 = \frac{\omega\mu_0}{2}\left[H_0^{(2)}(k_0R_+) + H_0^{(2)}(k_0R_-)\right] + \omega\mu_0\int_0^{\pi/2} d\varphi\, e^{-jk_0|z-z'|\sin\varphi} t(\rho(\varphi); x, x') + \omega\mu_0\int_{-j\infty}^0 d\varphi\, e^{-jk_0|z-z'|\sin\varphi} t(\rho(\varphi); x, x'). \tag{22}$$

The integrand in the third term of (22) decays and oscillates rapidly so that the integration may be completed period by period until the integral of the period around some φ_0 is under a given value ξ. For $\xi = 10^{-4}$, the typical value of φ_0 is about $5 \sim 6$ (radians).

We have represented the exterior electric field by the induced polarization source P through (15). To obtain the exterior magnetic fields, one starts from Maxwell's equations and gets

$$\omega\mu_0 H_x = -\beta_1 u_1(x) e^{-j\beta_1 z} + \omega \iint_{\Delta\Omega} dx' dz' P(x', z') \frac{\partial}{\partial z} G(x, z; x', z') \tag{23}$$

$$\omega\mu_0 H_z = j\frac{du_1(x)}{dx} e^{-j\beta_1 z} - \omega \iint_{\Delta\Omega} dx' dz' P(x', z') \frac{\partial}{\partial x} G(x, z; x', z'). \tag{24}$$

It remains to compute the far-field pattern associated with (7). By the saddle point method, we obtain the expression for the far field [9]:

$$\left|E_y^R(r, \theta)\right| \simeq \sqrt{\frac{k_0^2 - \rho^2}{k_0 r}} \cdot \begin{cases} \left|a_\rho(l)\right|, & 0 < \theta \leqslant \dfrac{\pi}{2} \\ \left|b_\rho(0)\right|, & \dfrac{\pi}{2} \leqslant \theta < \pi \end{cases} \qquad k_0 r \gg 1, \tag{25}$$

where $\rho = k_0 \sin\theta$ and (r, θ) are the polar coordinates of (x, z):

$$x = r\sin\theta \qquad z = r\cos\theta. \tag{26}$$

The quantities $a_\rho(l)$ and $b_\rho(0)$ are the coefficients of the radiation modes scattered to the forward and backward directions, respectively, which can be calculated from (11) and (12). It is noticed that (25) is the far field outside the slab waveguide, namely the radiation field, which does not include the scattered guided waves.

C. Numerical Procedure

The induced polarization source in (15), (23), and (24) is a function of the electric field in the irregular region $\Delta\Omega$, which may be represented by the undetermined nodal field values and the corresponding local bases in the finite

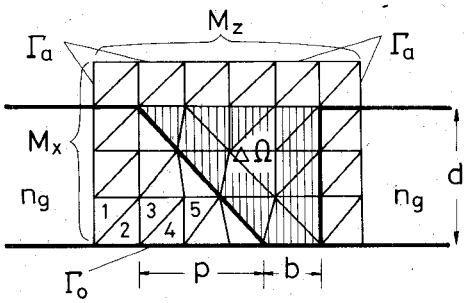

Fig. 2. Typical mesh division for linearly tapered discontinuity in slab waveguide.

element approach. With this in mind and by substituting (15), (23), and (24) into the exterior fields of (6), we finally obtain a functional of the form

$$I^a = \frac{j}{\omega\mu_0}\int_\Omega dv\left[\frac{\partial E_y^a}{\partial x}\frac{\partial E_y}{\partial x}+\frac{\partial E_y^a}{\partial z}\frac{\partial E_y}{\partial z}-k_0^2 n^2 E_y^a E_y\right] + \int_{\Gamma_a} ds f_h^a\left(E_y^a(\Delta\Omega)\right)\left[E_y(\Gamma^-)-f_e\left(E_y(\Delta\Omega)\right)\right] + \int_{\Gamma_a} ds E_y^a(\Gamma^-) f_h\left(E_y(\Delta\Omega)\right) - \int_{\Gamma_a} ds\left[E_{\text{inc}} f_h^a\left(E_y^a(\Delta\Omega)\right)+H_{\text{inc}}E_y^a(\Gamma^-)\right]. \quad (27)$$

In (27), f_e and f_h (or f_h^a) are the exterior electric and magnetic fields, respectively, which are all functions of E_y (or E_y^a) in $\Delta\Omega$. E_{inc} and H_{inc} are the incident tangential (to the boundary Γ_a) fields. It is noticed that the integrals on Γ_0 $(0 \leqslant z \leqslant l)$ of (6) vanish, since the Green's function is symmetric with respect to the $y-z$ plane and causes the tangential magnetic field on that boundary to be zero.

In the finite element solution, the region Ω is divided into a finite number of second-order triangular elements, each with six nodes [18]. A typical subdivision is shown in Fig. 2, where the intervals along the x and z axes are M_x and M_z, respectively. In order to avoid the singularities of Green's function, the artificial boundary Γ_a should enclose the boundary of the irregularities, as shown in Fig. 2.

Using the Ritz procedure [18], we finally obtain a matrix equation of the form

$$\bar{\bar{A}}\psi = s \quad (28)$$

in which $\bar{\bar{A}}$ represents a known matrix, while ψ and s are vectors concerning the unknown nodal values and the source terms due to the incident fields, respectively. The fields in Ω can be solved by inverting (28). The transmission coefficient T $(=a_1(l))$ and reflection coefficient R $(=b_1(0))$ as well as the radiation patterns are then obtained from (11), (12), and (25).

III. Numerical Results

Convergence of reflection and transmission coefficients for a linearly tapered air gap (Fig. 2 with $p=b=d$) is tabulated in Table I. The parameters of the slab are $k_0 d = 0.5$ and $n_g = 2.24$; thus only one guided mode can propagate in the waveguide. The field is incident from the left-hand side, which has a linearly tapered end. In the discontinuity region, there are $M_x - 1$ intervals along the x axis and $M_z - 2$ intervals along the z axis (referring to Fig. 2). Even for a rough division such as $M_x \times M_z = 2\times 4$, the relative errors are less than 0.2 percent.

TABLE I
Reflection and Transmission Coefficients of Linearly Tapered Air Gap (Fig. 2 with $p=b=d$) with $k_0 d = 0.5$ and $n_g = 2.24$

$M_x \times M_z$	R	T
2 × 4	0.4163 ∠102.98°	0.8792 ∠32.46°
3 × 6	0.4154 ∠102.85°	0.8797 ∠32.42°
4 × 8	0.4155 ∠102.87°	0.8795 ∠32.40°
5 × 9	0.4155 ∠102.87°	0.8795 ∠32.40°

TABLE II
Radiated Powers of Abruptly Terminated Air Gaps (Fig. 2 with $p=0$) with $k_0 d = 0.5$ and $n_g = 2.24$

b / d	$M_x \times M_z$	$1-\lvert R\rvert^2-\lvert T\rvert^2$	P_{RAD} / P_{INC}
1	4 × 5	0.0279	0.0279
2	4 × 7	0.0955	0.0955
3	4 × 9	0.1917	0.1918
4	4 × 10	0.3075	0.3075
5	4 × 10	0.4230	0.4229
6	4 × 10	0.5064	0.5064

Table II shows the radiated power of abruptly terminated air gaps (Fig. 2 with $p=0$) with various lengths. There are two methods for calculating the total radiated power: one is by subtracting the reflected and transmitted powers from the incident one, as shown in the third column of Table II; the other is by calculating the power radiated at each aspect angle θ and then integrating it through all θ $(0<\theta<\pi)$. The results of the latter method are shown in the last column of Table II. For most cases, the two methods give the same results up to four significant figures. The required CPU time depends on the mesh division in the irregular region. For example, the CPU times for $b/d=1$ $(M_x \times M_z = 4\times 5)$, $b/d=2$ $(M_x \times M_z = 4\times 7)$, and $b/d=3$ $(M_x \times M_z = 4\times 9)$ are 4.8, 10, and 18 minutes on the VAX 11/780, respectively.

Fig. 3 compares our results with those of Rozzi and In'tVeld [10] and Suzuki and Koshiba [14]. In our calculations, $M_x = 3$, while M_z is decided by the length of the gap. (Note that the dimension of the slab is smaller than

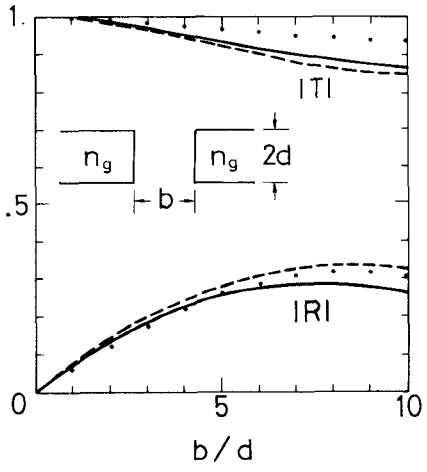

Fig. 3. Comparison of our results (———) with those of Rozzi *et al* [10] (••••) and Suzuki *et al.* [14] (– – – –). $p = 0$, $k_0 d = 0.2$, $n_g = 2.24$

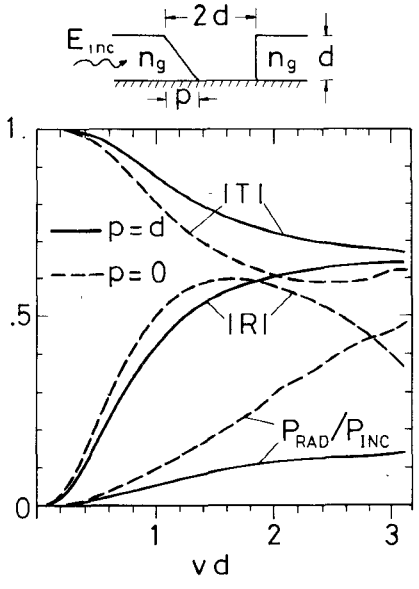

Fig. 4. Reflection and transmission coefficients as well as normalized radiated powers for linearly tapered air gaps. $vd = \sqrt{n_g^2 - 1} \cdot k_0 d$, $n_g = 2.24$.

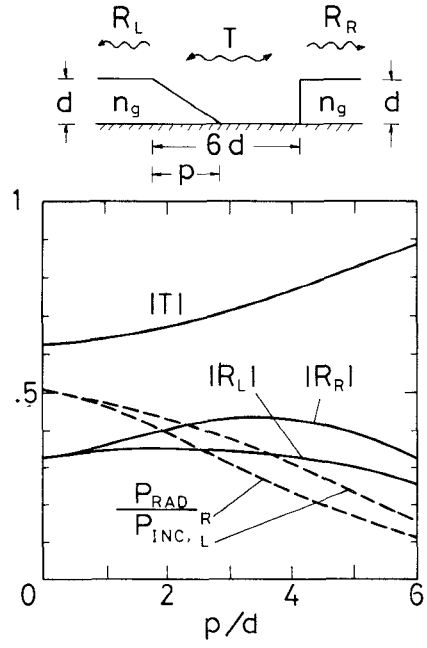

Fig. 5. Reflection and transmission coefficients as well as normalized radiated powers for incidence from LHS (with subscript L) and RHS (with subscript R). $k_0 d = 0.5$, $n_g = 2.24$

that of Tables I and II.) The curves show good agreement when b is small, and slight disagreement when b is increased.

The variations of reflection and transmission coefficients, as well as the normalized radiated power as a function of the normalized frequency, $vd = \sqrt{n_g^2 - 1} \cdot k_0 d$, are illustrated in Fig. 4. We show only the curves up to $vd = \pi$, beyond which the second guided mode of the uniform slab waveguide is above cutoff. We observe that the square sum of the reflection and transmission coefficients plus the normalized radiated power should equal unity for power conservation to hold at each normalized frequency vd. At lower frequencies ($vd < 0.32$), the three curves for $p = d$ have the same tendency as the corresponding ones for $p = 0$, probably due to the smaller taper length in comparison with the wavelength. As the frequency increases, the transmission coefficients for both discontinuities decrease (except near the cutoff of the second guided mode for the case of $p = 0$).

The behavior of the reflection coefficient in Fig. 4 is not as regular as that of the transmission coefficient. The reflection curve for $p = d$ is first less (for $vd < 1.84$) and then greater ($vd > 1.84$) than that for $p = 0$. The reason may be as follows: For $p = 0$ there are two abrupt junctions, which will cause strong reflection. For the normalized frequency in the middle range, the reflected waves from both junctions come approximately in phase and constructively add to yield the total reflected wave. But for the higher frequency such that the reflected waves from the two junctions add destructively, the total reflected wave may be reduced. On the other hand, in the case of $p = d$, the two ends of the air gap are different. The right-hand-side one is abrupt, which will cause strong reflection; while the left-hand-side one is tapered, which will cause less reflection, relatively. Therefore the total reflected wave is contributed mainly by the abrupt end only. This explains why the reflection curve for $p = d$ rises monotonically with increasing normalized frequency. It is noticed that the radiation loss for $p = 0$ is always greater than that for $p = d$.

Fig. 5 discusses the scattering behavior for waves incident from the left-hand side (LHS) and the right-hand side (RHS). For each p, the reflection coefficient (R_L) for incidence from the LHS is always less than that (R_R) from the RHS. A reasonable explanation is now suggested: In an air gap with (long) taper, the reflection is produced dominantly by the abrupt junction. For the field incident from the RHS, there is no power lost before it first meets the abrupt junction where a relatively large reflection take places. While the wave is incident from the LHS, it must

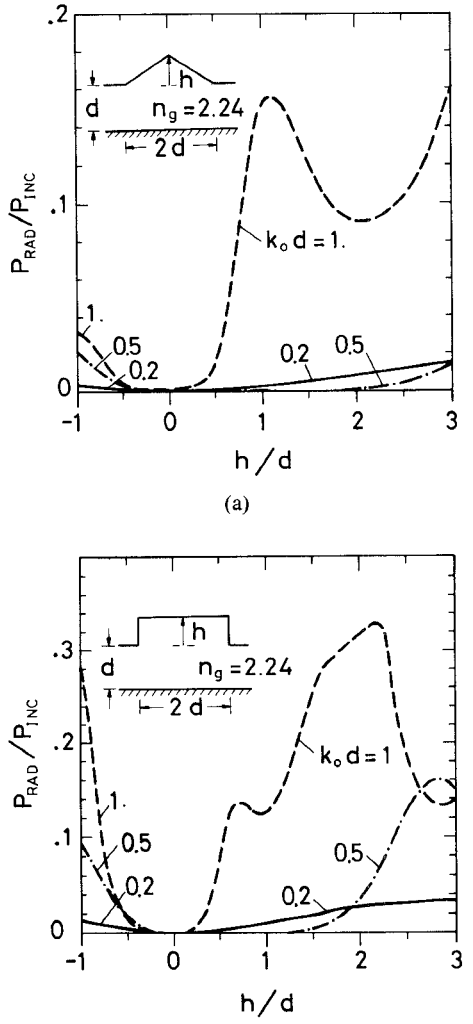

Fig. 6. Radiation losses due to fusion splices. (a) Triangular joint. (b) Rectangular joint.

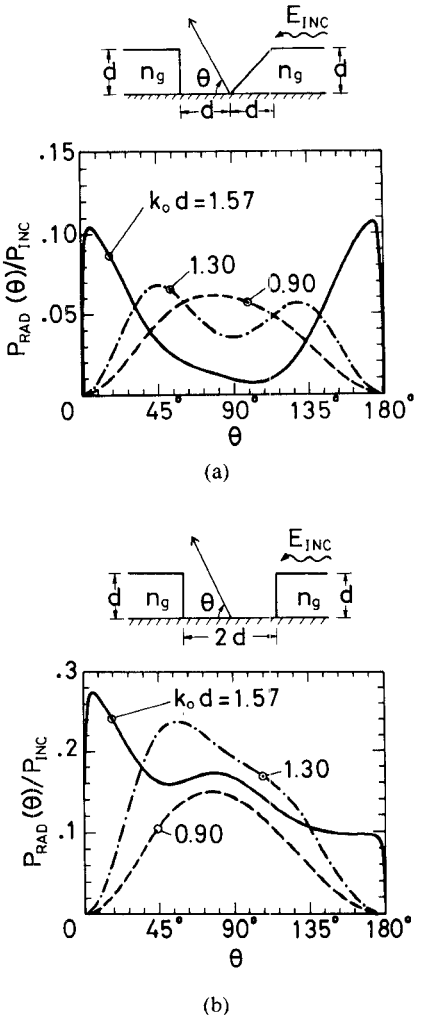

Fig. 7. Radiation patterns of (a) linearly tapered air gaps and (b) abruptly terminated air gaps. $n_g = 2.24$.

travel twice through the taper and free space, where some power is lost to the surroundings before it is reflected back to the LHS. Thus there is more reflected power for incidence from the RHS. Nevertheless the transmission coefficients for incidence from both sides should be the same by reciprocity.

The radiation loss due to fusion splices is illustrated in Fig. 6. Here we assume no refractive index change during splicing, but consider only the shape change. The waveguide is sunken for $h/d < 0$, and is raised for $h/d > 0$. We observed that the radiation loss of the rectangular splice (Fig. 6(b)) is greater than that of the triangular one (Fig. 6(a)). (Note the different scales in both figures.) One point worth noticing is that for $h/d > 0$, the losses for $k_0 d = 0.5$ are quite small until h is considerably large.

The radiation patterns of various discontinuities are plotted in Fig. 7(a) and (b) with $k_0 d$ as parameters. For $k_0 d \leqslant 0.9$, the radiation pattern has one single lobe with the maximum between $\theta = 80°$ and 90°, independent of the shape of the discontinuity. When $k_0 d$ becomes larger, the shape of the pattern changes. In the case of the abruptly terminated air gap (Fig. 7(b)), most of the lost power radiates in the direction of incidence. For the linearly tapered air gap (Fig. 7(a)), the power radiated to the vertical angle ($\theta = 90°$) is reduced, but is concentrated toward the two horizontal angles ($\theta = 0°$ and $\theta = 180°$).

IV. Conclusions

A new approach, which combines the partial variational principle (PVP), the finite element method coupled with frontal solution technique, and the Green's function technique, has been proposed to deal with discontinuity problems in a planar dielectric waveguide. Several numerical results, such as the reflection and transmission coefficients as well as the radiation losses and patterns, have been investigated and explained. In general the tapered structure increases the transmission coefficients but reduces the radiation losses. Also it changes the behavior of the reflection mechanism and the radiation patterns, which may be useful in designing related circuit components.

Due to its accuracy and generality, the proposed method can treat arbitrary discontinuities in a slab guide. This method can also solve the discontinuity problems with a

TM mode incidence. However if discontinuities are formed between two different slab guides, such as the step transformer, the present method will be inadequate because of the difficulty in constructing the Green's function. To solve this type of discontinuity, another method is under study and will appear in the near future.

Appendix
Derivation of (11) and (12)

For the system $(\boldsymbol{E}_1, \boldsymbol{H}_1; \boldsymbol{P})$ with $\boldsymbol{P}$ defined by (9) and a source-free system $(\boldsymbol{E}_2, \boldsymbol{H}_2)$, the Lorentz reciprocity relation takes the form

$$\int_0^\infty dx' \frac{\partial}{\partial z'}(\boldsymbol{E}_1 \times \boldsymbol{H}_2^* + \boldsymbol{E}_2^* \boldsymbol{H}_1)\cdot \hat{z} = -j\omega \int_0^\infty dx' \boldsymbol{P}\cdot \boldsymbol{E}_2^*. \tag{A1}$$

By representing the transverse components of $\boldsymbol{E}_1$ and $\boldsymbol{H}_1$ by (7) and (8), choosing either guided or radiation mode of the guide for $(\boldsymbol{E}_2, \boldsymbol{H}_2)$, and using the modal orthogonality property and the relations

$$a_\mu(z) = A_\mu(z) e^{-j\beta_\mu z}$$
$$b_\mu(z) = B_\mu(z) e^{j\beta_\mu z}$$

one has

$$\frac{dA_\mu}{dz'} = -\frac{j\omega}{2Y_{0\mu}} \int_0^\infty dx' P(x', z') u_\mu(x') e^{j\beta_\mu z'} \tag{A2}$$

$$\frac{dB_\mu}{dz'} = \frac{j\omega}{2Y_{0\mu}} \int_0^\infty dx' P(x', z') u_\mu(x') e^{-j\beta_\mu z'}. \tag{A3}$$

Then after integrating (A2) over $0 \leqslant z' \leqslant z$ and (A3) over $z \leqslant z' \leqslant l$, and then multiplying the results by $e^{-j\beta_\mu z}$ and $e^{j\beta_\mu z}$, respectively, one may obtain the desired expressions in (11) and (12).

Acknowledgment

The authors are deeply indebted to Dr. S. K. Jeng and Dr. R. B. Wu for providing computer subroutines and for valuable discussions.

References

[1] D. Marcuse, "Radiation losses of tapered dielectric slab waveguide," *Bell Syst. Tech. J.*, vol. 49, pp. 273–290, Feb. 1970.
[2] P. J. B. Clarricoats and A. B. Sharpe, "Modal matching applied to a discontinuity in a planar surface waveguide," *Electron. Lett.*, vol. 8, pp. 28–29, Jan. 1972.
[3] S. Miyanaga and T. Asakura, "Intensity profiles of outgoing beams from tapered grating couplers," *Radio Sci.*, vol. 17, pp. 135–143, Jan.–Feb. 1982.
[4] C. Brooke and M. Kharadhly, "Step discontinuities on dielectric waveguides," *Electron. Lett.*, vol. 12, pp. 471–473, Sept. 1976.
[5] T. Hosono, T. Hinata, and A. Inoue, "Numerical analysis of the discontinuities in slab dielectric waveguides," *Radio Sci.*, vol. 17, pp. 75–83, Jan.–Feb. 1982.
[6] S. F. Mahmoud and J. C. Beal, "Scattering of surface waves at a dielectric discontinuity on a planar waveguide," *IEEE Trans. Microwave Theory Tech.*, vol. MTT-23, pp. 193–198, Feb. 1975.
[7] K. Morishita, S.-I. Inagaki, and N. Kumagai, "Analysis of discontinuities in dielectric waveguides by means of the least squares boundary residual method," *IEEE Trans. Microwave Theory Tech.*, vol. MTT-27, pp. 310–315, Apr. 1979.
[8] H. Shigesawa and M. Tsuji, "Mode propagation through a step discontinuity in dielectric planar waveguide," *IEEE Trans. Microwave Theory Tech.*, vol. MTT-34, pp. 205–212, Feb. 1986.
[9] T. E. Rozzi, "Rigorous analysis of the step discontinuity in a planar dielectric waveguide," *IEEE Trans. Microwave Theory Tech.*, vol. MTT-26, pp. 738–746, Oct. 1978.
[10] T. E. Rozzi and G. H. In'tVeld, "Field and network analysis of interacting step discontinuities in planar dielectric waveguides," *IEEE Trans. Microwave Theory Tech.*, vol. MTT-27, pp. 303–309, Apr. 1979.
[11] T. E. Rozzi and G. H. In'tVeld, "Variational treatment of the diffraction at the facet of d.h. lasers and of dielectric millimeter wave antennas," *IEEE Trans. Microwave Theory Tech.*, vol. MTT-28, pp. 61–73, Feb. 1980.
[12] P. Gelin, S. Toutain, and J. Citerne, "Scattering of surface waves on transverse discontinuities in planar dielectric waveguides," *Radio Sci.*, vol. 16, pp. 1161–1165, Nov.–Dec. 1981.
[13] C. N. Capsalis, J. G. Fikioris, and N. K. Uzunoglu, "Scattering from an abruptly terminated dielectric-slab waveguide," *J. Lightwave Tech.*, vol. LT-3, pp. 408–415, Apr. 1985.
[14] M. Suzuki and M. Koshiba, "Finite element analysis of discontinuity problems in a planar dielectric waveguide," *Radio Sci.*, vol. 17, pp. 85–91, Jan.–Feb. 1982.
[15] S.-J. Chung and C. H. Chen, "Partial variational principle for electromagnetic field problems: Theory and applications," *IEEE Trans. Microwave Theory Tech.*, vol. 36, pp. 473–479, Mar. 1988.
[16] E. Hinton and D. R. J. Owen, *Finite Element Programming*. New York: Academic Press, 1977.
[17] T. Tamir, Ed., *Integrated Optics*, *Topics in Applied Physics*, (2nd ed.) New York: Springer–Verlag, 1979.
[18] O. C. Zienkiewicz, *The Finite Element Method*. New York: McGraw–Hill, 1977.

Shyh-Jong Chung was born in Taipei, Taiwan, Republic of China, on January 18, 1962. He received the B.S.E.E. degree in June 1984, and the Ph.D. degree in July 1988, both from National Taiwan University, Taipei, Taiwan. His topics of interest include waveguide discontinuity problems, integrated optics, wave propagation, and numerical techniques in electromagnetics.

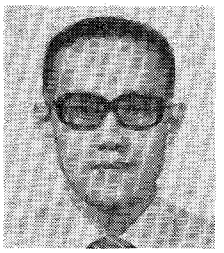

Chun Hsiung Chen was born in Taipei, Taiwan, Republic of China, on March 7, 1937. He received the B.S.E.E. degree from National Taiwan University, Taipei, Taiwan, in 1960, the M.S.E.E. degree from National Chiao Tung University, Hsinchu, Taiwan, in 1962, and the Ph.D. degree in electrical engineering from National Taiwan University in 1972.

In 1963 he joined the faculty of the Department of Electrical Engineering, National Taiwan University, where he is now a Professor. From August 1982 to July 1985 he was Chairman of the department. In 1974 he was a Visiting Researcher for one year at the Department of Electrical Engineering and Computer Sciences, University of California, Berkeley. From August 1986 to July 1987, he was a Visiting Professor at the Department of Electrical Engineering, University of Houston, TX. His areas of interest include antenna and waveguide analysis, propagation and scattering of waves, and numerical techniques in electromagnetics.